Asian Journal of Chemistry; Vol. 38, No. 5 (2026), 1142-1152
ASIAN JOURNAL OF CHEMISTRY
https://doi.org/10.14233/ajchem.2026.35539

Aggregation, Photo-Isomerisation and Antibacterial Behaviour of Adamantane based Zinc Azo Schiff base Complex

V. VEERA MUTHAMMAL[1], N. VASIMALAI[1], SUNDAR MANICKAM[2] and S. KUTTI RANI[1,*]

[1]Department of Chemistry, B.S. Abdur Rahman Crescent Institute of Science and Technology, Vandalur, Chennai-600048, India
[2]Research & Development, Allastir Pvt. Ltd., SIDCO Industrial Estate, Vichoor, Manali New Town, Chennai-600103, India

*Corresponding author: E-mail: skrani@crescent.education

Received: 29 December 2025 *Accepted*: 9 March 2026 *Published online*: 4 May 2026 AJC-22338

A new adamantane-based azo-Schiff base ligand (AADSB) and its zinc(II) complex (ZnAADSB) were synthesized and characterized to investigate their structural, photophysical, and antibacterial properties. The ligand was prepared by condensation of an azo-salicylaldehyde precursor with adamantylamine, followed by coordination with zinc chloride to yield the corresponding complex. The structural confirmation was achieved using FT-IR, UV–Vis, $^{1}H/^{13}C$ NMR, ESI-MS, elemental analysis, FE-SEM, EDX, thermal analysis and fluorescence spectroscopy, indicating coordination through N,O-donor sites. The complex ZnAADSB exhibited solvent-dependent fluorescence behaviour. In chloroform, the complex showed aggregation-induced emission enhancement (AIEE) with gradual addition of DMSO, while higher DMSO fractions caused fluorescence quenching. Aggregate formation was supported by ^{1}H NMR and dynamic light scattering studies, which revealed increased particle size. The complex did not show reversible photoisomerisation under UV irradiation (365 nm), likely due to steric hindrance from the adamantane unit. Antibacterial activity of the ligand and its Zn complex was evaluated against Gram-negative (*Escherichia coli* and *Salmonella enterica*) and Gram-positive (*Staphylococcus aureus* and *Bacillus subtilis*) bacteria using agar well diffusion, MIC and MBC methods. The zinc complex consistently outperformed the free ligand. At 1000 µg/mL, ZnAADSB showed inhibition zones of 22.37 ± 0.25 mm (*E. coli*), 21.47 ± 0.43 mm (*S. aureus*), 18.55 ± 0.31 mm (*S. enterica*), and 16.10 ± 0.17 mm (*B. subtilis*).

Keywords: *p*-Toluidine, Schiff base, Zn complex, Photo-isomerisation, Antimicrobial activity.

INTRODUCTION

The rapid emergence and dissemination of drug-resistant microorganisms have significantly compromised the effectiveness of current therapies for infectious diseases, creating a serious global healthcare challenge associated with increased morbidity and mortality [1]. Consequently, the search for new antimicrobial agents with improved efficacy and novel mechanisms of action has become a major research priority. Among the compounds investigated for this purpose, Schiff bases and their metal complexes have attracted sustained attention due to their facile synthesis, structural diversity and broad biological potential [2].

Azo-Schiff bases, containing both azo (–N=N–) and azomethine (–CH=N–) functionalities, represent an important class of multifunctional organic molecules. The coexistence of these donor groups often enhances their coordination ability and contributes to diverse pharmacological properties, including antibacterial, antifungal and antitumor activities [2]. In addition to biomedical relevance, azo-containing systems are widely recognized for their optical and electronic characteristics, making them useful in solar energy conversion, sensing devices, nonlinear optics and molecular data storage applications [3].

Schiff base ligands are particularly valuable in coordination chemistry since the azomethine nitrogen can strongly bind metal ions, generating stable complexes with tunable physicochemical properties [4]. Incorporation of metal ions frequently improves lipophilicity, redox behaviour and biological activity relative to the parent ligands. Among biologically relevant metals, zinc(II) is especially attractive since it plays essential roles in more than 300 enzymatic systems and exhibits favourable biocompatibility with relatively low toxicity [5,6]. Zinc complexes of Schiff bases have therefore been widely explored as potential therapeutic and functional materials.

This is an open access journal, and articles are distributed under the terms of the Attribution 4.0 International (CC BY 4.0) License. This license lets others distribute, remix, tweak, and build upon your work, even commercially, as long as they credit the author for the original creation. You must give appropriate credit, provide a link to the license, and indicate if changes were made.

Azobenzene and related azo derivatives are also known for reversible photoisomerisation between thermodynamically stable *trans*- and metastable *cis*-forms under light irradiation [7-10]. This light-responsive behaviour has stimulated interest in photochromic and stimuli-responsive materials for smart optoelectronic devices and chemosensors [11-15]. Furthermore, azo-Schiff bases may exhibit tautomeric equilibria such as azo-imine ⇌ hydrazone-imine or azo-imine ⇌ azo-amine forms, which can influence their electronic absorption, fluorescence and coordination behaviour [16,17]. However, studies addressing the luminescent and aggregation-related properties of such systems remain comparatively limited [18-22].

In view of these considerations, the present work focuses on the synthesis of a new adamantane-containing azo-Schiff base ligand and its zinc(II) complex, followed by comprehensive structural characterization (FT-IR, UV/Vis, NMR, elemental analysis) and evaluation of their photophysical and antibacterial properties. The influence of zinc coordination on the aggregation behaviour, fluorescence response and antimicrobial efficacy was also investigated.

EXPERIMENTAL

All reagents and chemicals used in this study were procured from commercial vendors (BLD China, Spectrochem, SRL Chemicals and Hyma Chemicals) and employed without further purification. All the solvents used for the synthesis were of AR grade and used as such. All the reactions were carried out in nitrogen atmosphere. *E*-2-Hydroxy-5-(*p*-tolyldiazenyl)benzaldehyde was synthesised by conventional diazotisation reaction using *p*-toluidine and 2-hydroxybenzaldehyde. Biological studies related chemicals such as Nutrient broth, Nutrient agar, Muller Hinton agar, sodium chloride and DMSO were purchased from HiMedia Laboratories, LLC.

Synthesis of ligand AADSB: 2-Hydroxy-5-[(*E*)-(4-methylphenyl)diazenyl]benzaldehyde (1.0 g, 1.16 mmol) was dissolved in dimethyl sulfoxide (10 mL) to afford a limpid solution. To the solution, adamantylamine hydrochloride (0.94 g, 5.0 mmol) was dissolved in methanol (5 mL) was added triethylamine (0.76 g, 7.5 mmol) and the reaction was stirred for 12 h at 75 ºC followed by the addition of crushed ice which resulted in the formation of adamantane condensed azo Schiff base (AADSB) as yellow solid. The product was filtered, washed with methanol and dried at 55 ºC under vacuum for 8 h to get pale orange colour solid (**Scheme-I**). Yield: 1.3 g, 84%; ^{1}H NMR (400 MHz, $CDCl_3$, δ ppm): 1.62-1.73 (m, 6H; $CH_{2\,(adam\text{-}a,e)}$), 1.835 (d, 6H; $CH_{2(adam)}$), 2.15 (m, 3H; $CH_{(adam)}$), 2.34 (s, 3H; $-CH_3$), 6.90 (d, J_{HH} = 9.2Hz, 1H; ArH), 7.22 (d, J_{HH} = 8.4, 2H; ArH), 7.70 (d, J_{HH} = 8.4, 2H; ArH), 7.78 (d, J_{HH} = 2.4, 1H; ArH), 7.90, (dd, J_{HH} = 11.6, 1H; ArH), 8.26, (s, 1H, -CH=N-), 15.07 (s, 1H, -OH); ^{13}C NMR (125 MHz, $CDCl_3$, δ ppm): 21.48, 29.27, 36.07, 42.75, 56.95, 116.87, 120.29, 122.42, 127.12, 129.03, 129.72, 140.48, 143.87, 150.83, 159.40, 169.86. ESI-MS: Calcd. *m/z* = 373.215 Da; Obsd. *m/z* 374.223 Da $[M+H]^+$.

Synthesis of Zn complex: Ligand AADSB (1.0 g, 2.6 mmol) was dissolved in 10 mL of DMSO followed by the addition of 0.32 g of KOH and zinc chloride (0.21 g, 1.2 mmol) dissolved in methanol and then the whole mixture was charged immediately. The reaction admixture was subjected to a thermal regimen of 85 ºC, sustained over a duration of 8 h. Following the 8 h of stirring, the reaction mixture was added dropwise to the crushed ice to isolate the product, which was filtered, washed with methanol and finally dried for 8 h to obtain dark orange colour solid (ZnAADSB) complex (**Scheme-I**). Yield: 1.53 g, 85%. ^{1}H NMR (400 MHz, $CDCl_3$, δ ppm): 1.49 (m, 3H, CH_{adam}), 1.57-1.71 (m, 6H, $CH_{2\,(adam\text{-}a,e)}$), 1.94 (m, 3H, $CH_{2(adam)}$), 2.04 (m, 3H, $CH_{(adam)}$), 2.35 (s, 3H, $-CH_3$), 6.87 (d, J_{HH} = 9.2Hz, 1H; ArH), 7.22 (d, J_{HH} = 8.4, 2H, ArH), 7.69 (d, J_{HH} = 8.0, 2H, ArH), 7.77 (d, J_{HH} = 2.4, 1H, ArH), 7.92, (dd, J_{HH}= 11.6, 1H, ArH), 8.35, (s, 1H, -CH=N-); ^{13}C NMR (125 MHz, $CDCl_3$, δ ppm): 21.46, 29.57, 35.88, 43.41, 60.21, 117.77, 122.22, 124.15, 128.26, 129.70, 133.76, 140.06, 142.49, 151.01, 166.66, 172.92. ESI-MS: calcd. *m/z* = 810.365 Da, found *m/z* 814.593 Da $[M+4H]^+$.

Aggregation study: A stock solution of ZnAADSB complex was prepared by dissolving 54 mg of compound in 100 mL of chloroform, resulting in a concentration of 0.66 mM. From this stock, 2.5 mL was withdrawn and diluted to 50 mL with chloroform to obtain a working solution of 33 μM. All solutions were prepared freshly prior to the experimental analysis. In aggregation studies, above 33 μM solution and DMSO solvent was taken as stock. From this stock, three different volume ratios were prepared *viz*. (i) 8 mL of Zn complex with 2 mL of DMSO; (ii) 5 mL of Zn complex with 5 mL of DMSO and; (iii) 2 mL of Zn complex with 8 mL of DMSO.

Photo-isomerisation study: A stock solution of Zn complex was prepared by dissolving 54 mg of compound in 100 mL of chloroform, resulting in a concentration of 0.66 mM. From this stock, 2.5 mL was withdrawn and diluted to 50 mL with chloroform to obtain a working solution of 33 μM. All solutions were prepared freshly prior to the experimental analysis.

Biological studies: Tested strains, namely *Escherichia coli* MTCC 443, *Staphylococcus aureus* MTCC 2940, *Salmonella enterica* MTCC 9844 and *Bacillus subtilis* MTCC 441, were employed in accordance with the directives delineated by the Clinical and Laboratory Standards Institute (CLSI) [23]. The bacterial strains were cultivated in nutrient-rich broth and subjected to incubation at 37 ºC for a temporal span of 24 h. Each bacterial strain was procured from the Microbial Type Culture Collection and Gene Bank (MTCC), Chandigarh, India.

Antibacterial assay: The antibacterial activity of ligand AADSB and its Zn(II) complex was evaluated by the agar well diffusion method. Bacterial suspensions adjusted to 0.5 McFarland standard (approximately 10^6 CFU/mL) were uniformly spread on Mueller-Hinton agar plates using sterile swabs. Wells of 8 mm diameter were prepared and test samples at different concentrations (1000, 500, 250 and 100 μg/mL) were introduced into the respective wells. Ciprofloxacin (30 μg/mL) was used as the positive control. Plates were allowed to pre-diffuse for 15 min at room temperature and then incubated at 37 ºC for 24 h. Antibacterial activity was determined by measuring the zone of inhibition (ZOI) in millimetres [24]. All experiments were carried out in triplicate and results were expressed as mean ± standard deviation.

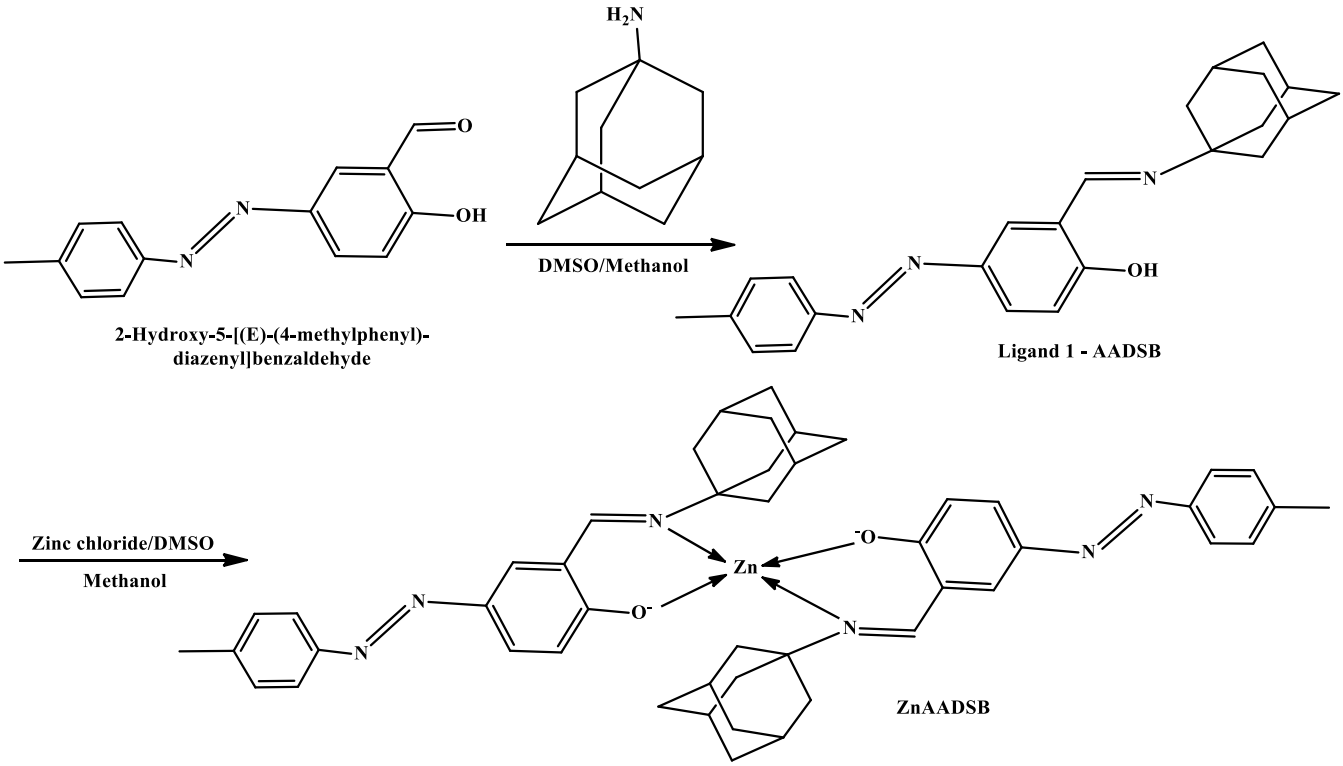

Scheme-I: Synthetic scheme for the synthesis of ligand AADSB and ZnAADSB

Minimum inhibitory concentration (MIC) was determined by the broth microdilution method using sterile 96-well microplates. Serial dilutions of the test samples (1000-7.812 µg/mL) were prepared in Mueller-Hinton broth, followed by inoculation with bacterial suspension. Negative and sterility controls were included. After incubation at 37 ºC for 18-24 h, MIC values were recorded as the lowest concentration showing no visible bacterial growth, as confirmed using an ELISA plate reader (Tecan Infinite F50 Plus). Minimum bactericidal concentration (MBC) was defined as the lowest concentration resulting in bacterial death. All measurements were performed in triplicate and reported as mean ± standard deviation.

RESULTS AND DISCUSSION

The synthesis of the adamantane-based azo-Schiff base zinc complex was accomplished in two sequential steps, as outlined in **Scheme-I**. Initially, condensation of 1-amino-adamantane hydrochloride with the corresponding azo-salicyl-aldehyde derivative afforded the Schiff base ligand AADSB. Subsequently, AADSB acted as a bidentate ligand and reacted with zinc chloride at 85 ºC to obtain the Zn(II) complex (ZnAADSB) in 85% yield. The overall yield for the two-step process was 72%. Both AADSB and ZnAADSB were stable toward air and moisture. In addition, they showed good solubility in polar protic and aprotic solvents, with limited solubility in non-polar media. The formation and purity of the derived compounds were confirmed by ^{1}H & ^{13}C NMR, FT-IR and mass spectrum.

NMR spectral studies: From the ^{1}H NMR spectrum of ligand (Fig. 1a), the spectrum reveals the Schiff base formation due to the sharp singlet at δ 8.262 ppm for (-C=N-) azomethine proton [25]. This is also accompanied by the phenolic hydroxy proton (-OH) at δ 15.079 ppm. Aromatic protons of the ligands were observed in region between δ 6.883-7.912 ppm [26] and the CH_3- of *p*-tolyl group was observed as a strong singlet at δ 2.349 ppm. The aliphatic protons of the adamantane moiety exhibited characteristic splitting patterns. The three bridge-head methine (CH) protons appeared as a multiplet at δ 2.150 ppm, whereas the methylene (CH_2) protons were resolved into two distinct environments. One set appeared as doublets at δ 1.835 ppm, while the second set was observed as doublet of doublets in the δ 1.629-1.730 ppm region, reflecting the rigid cage-like structure of the adamantane unit.

The ^{1}H NMR spectrum of ZnAADSB (Fig. 1b) indicates the azomethine proton showed slightly upshift at δ 2.353 ppm and disappearance of phenolic –OH proton also confirms the complexation with zinc ions through N-O coordinating sites [27]. Other aromatic protons did not show considerable shifts but the aliphatic protons in adamantine moiety shows a significant splitting after complexion. The three protons of sp^3-CH group show multiplet as same as ligand AADSB (Fig. 2a) whereas the 12 protons of sp^3-CH_2 groups shows doublets as shown in the Fig. 2b. The change is splitting patterns may be attributed to the spatial arrangement of adamantine groups in complex.

The ^{13}C NMR of ligand AADSB and its ZnAADSB complex are shown in the Fig. 3. In the ^{13}C NMR of the ligand, δ 21-56 ppm is assigned to aliphatic groups of the ligands whereas δ 116-159 ppm assigned to carbons of the aromatic rings and phenolic carbon is observed at δ 169 ppm [28]. In complex, there is not much change in shift is observed except carbon connected to the ligating sites. The change in

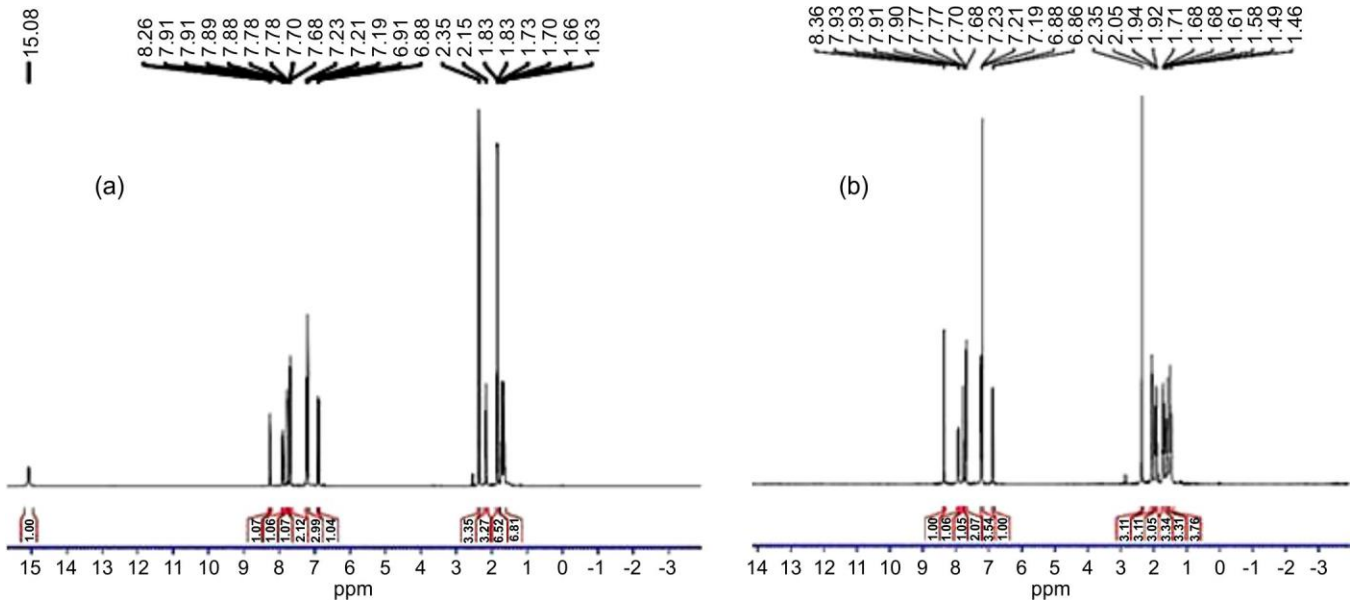

Fig. 1. [1]H NMR spectra of (a) ligand AADSB and (b) ZnAADSB

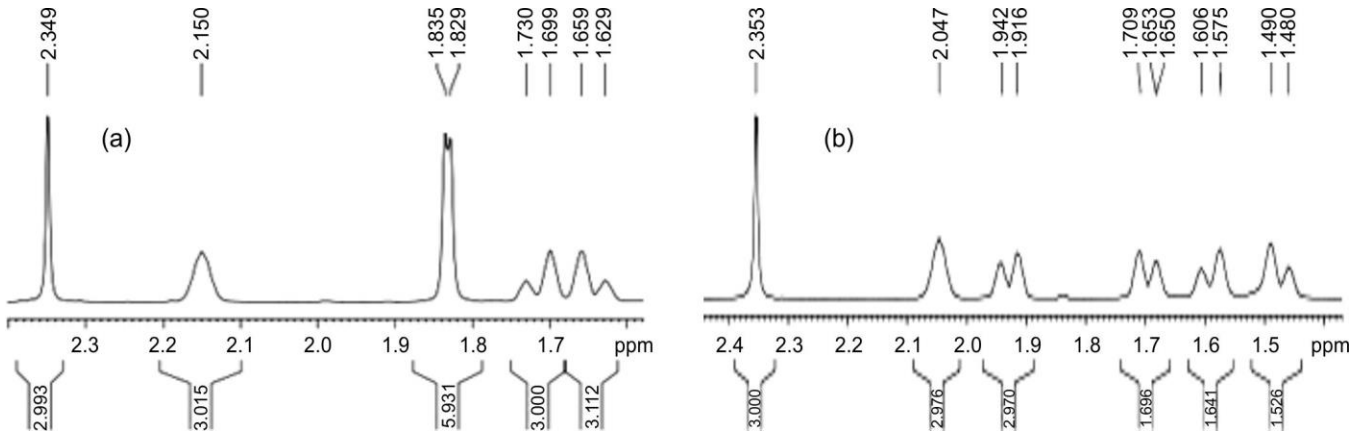

Fig. 2. Selected region of [1]H NMR spectra (a) ligand AADSB and (b) ZnAADSB

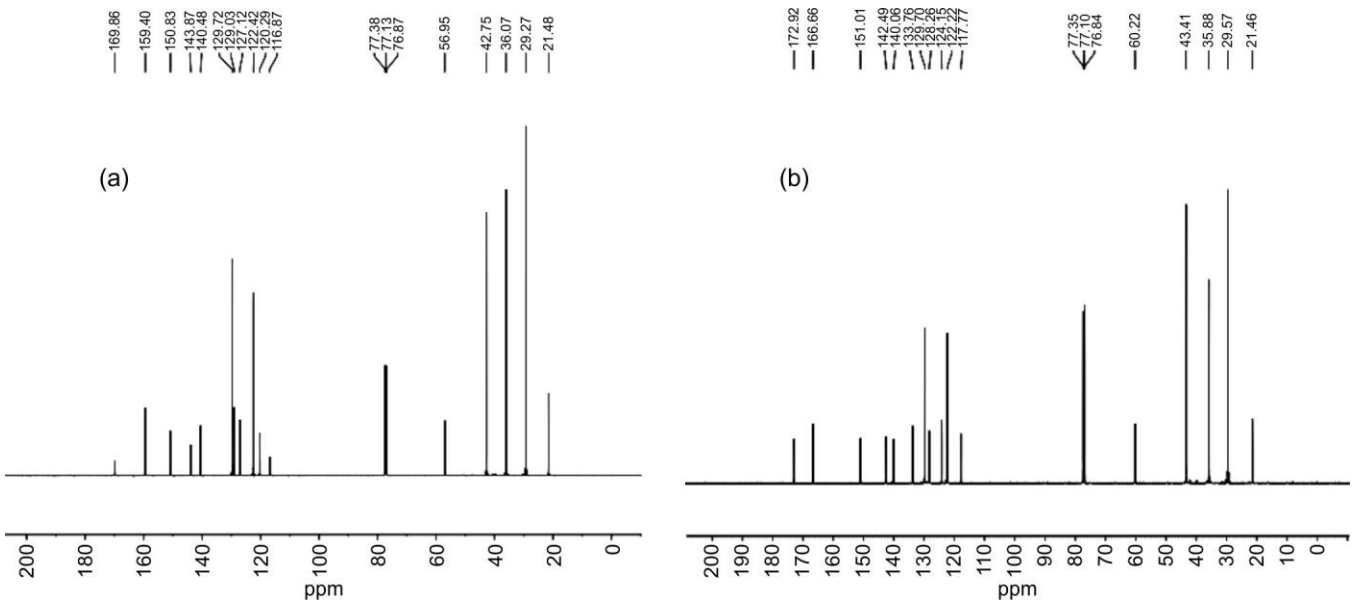

Fig. 3. [13]C NMR spectra of (a) ligand AADSB and (b) ZnAASDB complex

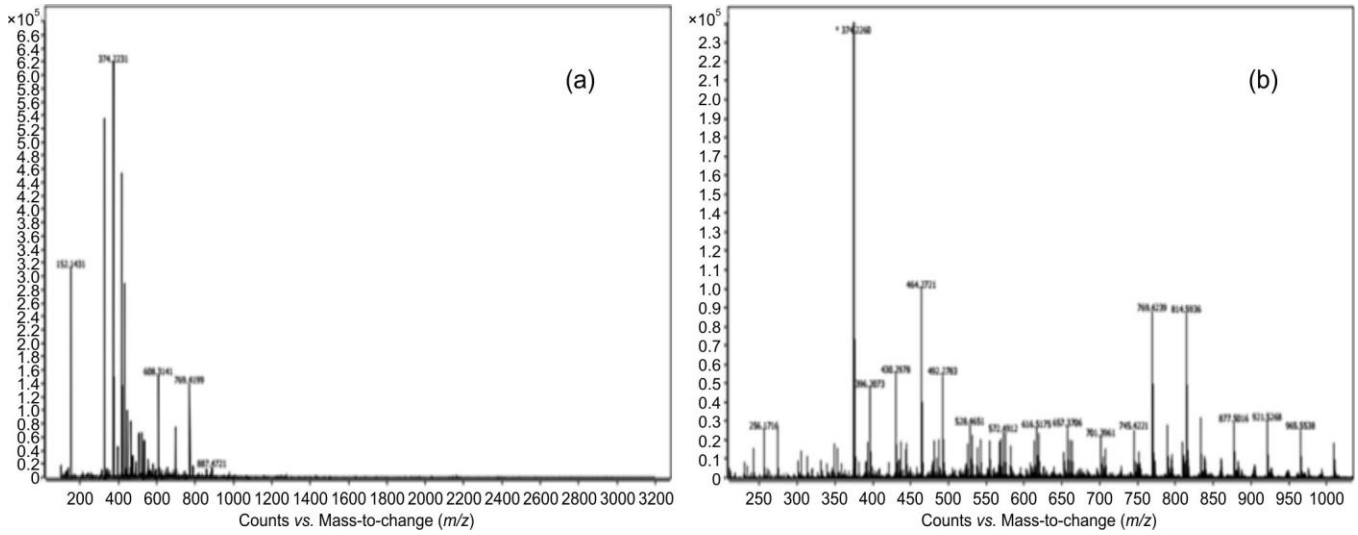

Fig. 4. (a) HRMS spectrum of ligand AADSB and (b) ESI-MS spectrum of ZnAADSB

shifts of δ 7.26 ppm in aldimine carbon (C=N) shows the coordination of zinc in a complex. Also, the carbon of phenoxide anion and sp^3-C of adamantine group (=N-C_{adam}) shows a variation of δ 3.06 and δ 3.27 ppm, respectively.

Mass studies: The structures of ligand and its Zn complex were also confirmed by positive-ion ESI mass spectra shown in Fig. 4a-b. For AADSB, two peaks were observed at *m/z* 374.22 and 769.41 whose fragmentations coincides with $[M+H]^+$ and $[2M+Na]^+$, respectively. The calculated values of fragments were *m/z* 373.22 and 769.41, respectively, which are in good agreement with the measured values ligand AADSB. Similarly, calculated molecular ion peak of ZnAADSB is *m/z* 810.36 whereas the peak was observed at *m/z* 814.59, which corresponds to a $[M+4H]^+$ peak.

FT-IR studies: The FT-IR spectra of ligand AADSB and its ZnAADSB complex are shown in Fig. 5a-b. The strong peak at 1620 cm^{-1} confirms the presence of ν(-C=N-) imine bond of the Schiff base [29]. This peak is slightly shifted to 1605 cm^{-1} after complexation with zinc ion. A shoulder peak at 1526 cm^{-1} indicates the presence of azo groups in the ligand which clearly visible as a weak peak at 1527 cm^{-1} in the complex. The change in stretching vibrations of ν(-C_{ada}-N-) and ν(-C_{arom}-N-) clearly indicates the coordination of zinc ions as Zn-N-O with the ligands. Within the ligand, prominent peaks were discerned at 2847 and 2911 cm^{-1}, validating the asymmetric and symmetric stretching vibrations of ν(-CH_2-) groups inherent to the adamantane moieties; conversely, the complex manifested a relative stasis in observed spectral shifts. The stretching vibrations of aromatic ν(=CH_{arom}) observed at 3046 cm^{-1} in the ligand was shifted to 3030 cm^{-1} in the complex [30]. In complex, the peaks at 512 and 465 cm^{-1} referring to Zn-O and Zn-N vibrations in Zn-N-O coordination sites were observed, respectively.

Morphological studies: The FE-SEM images and EDX analysis of ligand and its Zn complex are shown in Fig. 6a-b. Fig. 6a shows the cube shaped morphology with various dimensions while after complexion with Zn (Fig. 6b), the morphology exhibits the densely packed aggregates of irregular shapes. The EDX mapping showed the constructing block

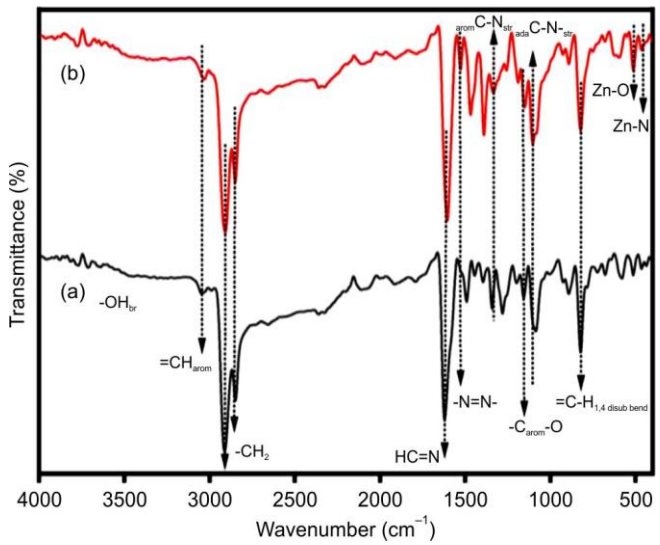

Fig. 5. FTIR spectra of (a) ligand AADSB and (b) ZnAADSB

elements like carbon, nitrogen and oxygen for ligand (inset of Fig. 6a) while Zn as an added element for Zn complex (inset Fig. 6b).

Thermal studies: Thermal analysis (Fig. 7) showed minor weight loss below 200 ºC, indicating trace moisture or adsorbed solvent in both the ligand and its Zn complex [31]. The real decomposition (step 1) of the ligand occurs between 200-350 ºC with a major weight loss of 46.92%, which indicates the partial breakdown of the ligand structure. Upon further heating, a 23.27% weight loss was observed between 350-800 ºC (step 2), attributed to decomposition of residual ligand fragments, leaving 30% residue. Similarly, when compared with that of ligand AADSB, Zn complex also exhibits similar degradation pattern with 32.8% weight loss in step 1 followed by same weight loss in step 2 with increased residue weight (45%).

Optical studies: The UV-visible spectra of ligand (73 μM) and its Zn complex (33 μM) were recorded in coordinating and non-coordinating solvents like chloroform and DMSO solvents are shown in Fig. 8. The UV-visible spect-

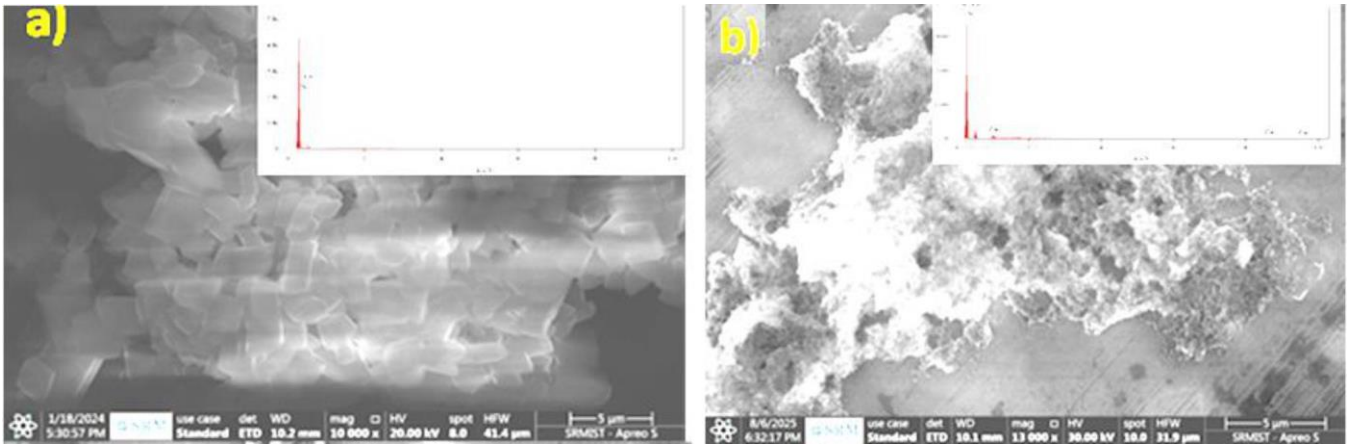

Fig. 6. FE-SEM images of (a) ligand AADSB and (b) ZnAADSB complex

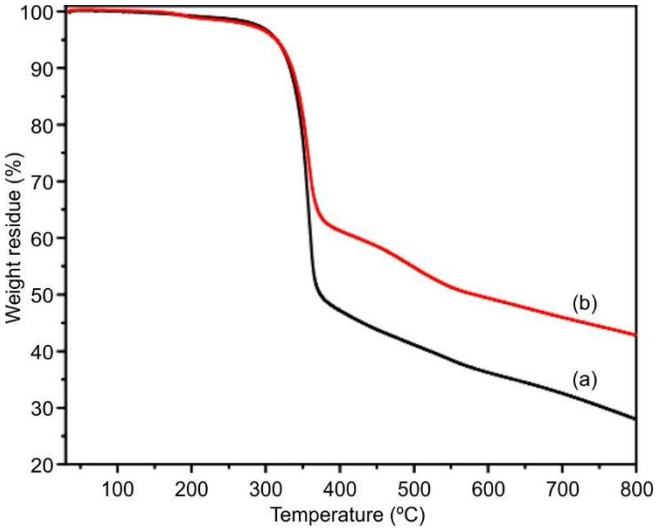

Fig. 7. TGA curves of (a) ligand AADSB and (b) ZnAADSB complex

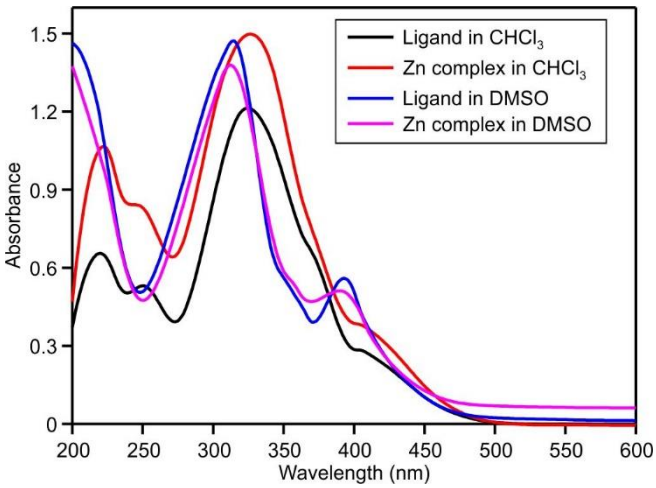

Fig. 8. UV-Visible spectra of ligand AADSB and ZnAADSB complex in chloroform and DMSO solvents

rum of the ligand in chloroform exhibited absorptions at 220, 250 nm [31] corresponds to aromatic -C=C- π-π*, transitions, 325 nm assigned for n- π* transitions of –C=N- chromophore [32] and a further absorption at 405 nm for –N=N- azo chromophore. A small shift in absorption wavelength indicates the coordination of ligand to zinc ions. The corresponding shift in n-π* was also observed. A hypsochromic shift for ligand and complex in DMSO for both the transitions is observed [33]. This blue shift is mainly attributed the formation of Zn DMSO adduct in DMSO solvent. More interestingly, a clear and sharp peak of n-π* related –N=N- azo chromophore was observed.

In the fluorescence study, the excitation of ligand AADSB ($CHCl_3$) at λ_{ex} 425 nm gives the emission peak λ_{em} at 501 whereas the ZnAADSB complex displays two emission wavelength λ_{em} at 483 and 511 nm [34]. The same trend is observed in coordinating solvents, DMSO, with blue shift in emission wavelength. In DMSO, excitation wavelength λ_{ex} at 390 nm shows a single emission peak at λ_{em} 476 nm whereas for Zn AADSB complex two emission peaks λ_{em} at 437 and 495 nm were observed (Fig. 9). Moreover, the fluorescence quenching was observed for both the ligand and its Zn complex in the coordinating solvent, mainly due to coordination of DMSO to Zn ions, which altered the position and intensity of the emission spectra.

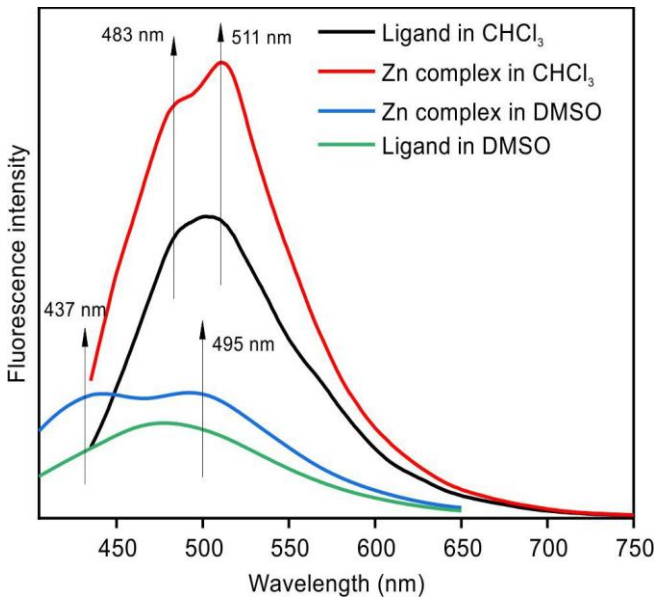

Fig. 9. Fluorescence spectra of ligand AADSB and ZnAADSB complex in chloroform and DMSO solvents

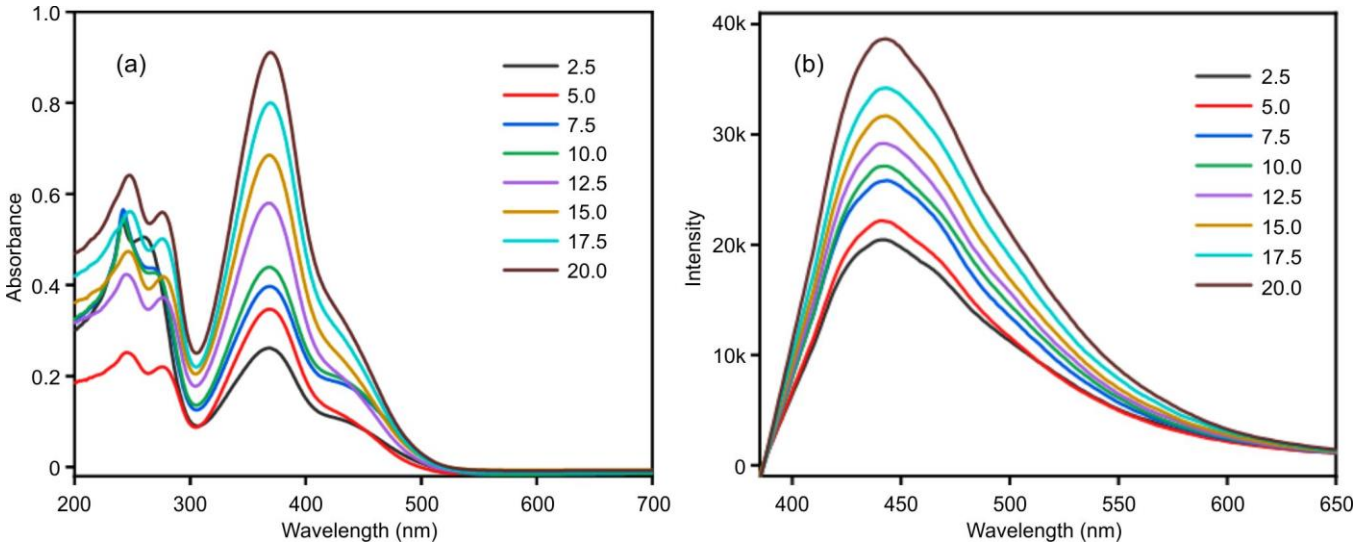

Fig. 10. (a) UV-Visible and (b) fluorescence spectra of ZnAADSB complex ($CHCl_3$) with increasing concentration

The absorption and fluorescence spectra were ascertained for quinine sulphate and a zinc complex, as shown in Fig. 10. Fig. 11 elucidates the correlation between relative absorbance and integrated fluorescence intensity for both quinine sulphate and the zinc complex.

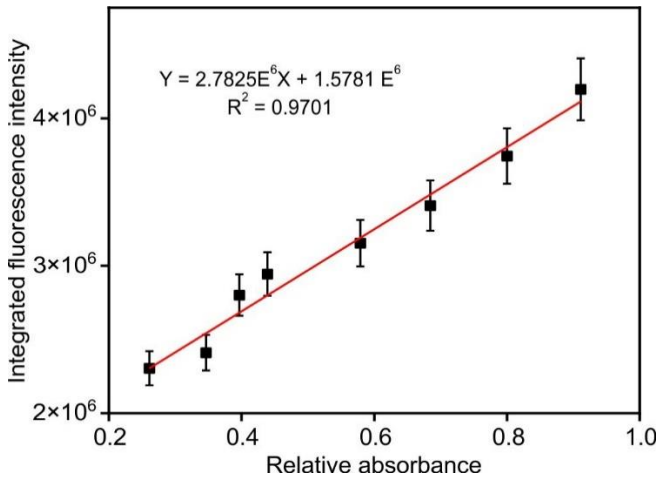

Fig. 11. Quantum yield plot of ZnAADSB complex

The fluorescence quantum yield of the zinc complex was ascertained *via* the subsequent eqn. 1 [35]:

$$QY_{Zn} = F_{Zn} \times As \times \frac{QYs}{Fs} \times A_{Zn} \quad (1)$$

where A_{Zn} denotes the excitation wavelength of zinc complex (370 nm); F_{Zn} denotes the integrated fluorescence emission area of zinc complex (414,321); QYs indicates the quantum yield of standard quinine sulphate (54%); As represents the excitation wavelength of quinine sulphate (250 nm); Fs corresponds to the integrated fluorescence range of quinine sulphate (1,266,010); and QY_{Zn} means the fluorescence quantum yield of zinc complex, calculated as 28.1%.

Aggregation behaviour studies: In-order to check the aggregation induced emission enhancement, the experiment was performed with increasing concentration of coordinating solvents, *i.e.* DMSO. From the Fig. 12, the 375 nm excitation of ZnAADSB complex in chloroform shows the emission maximum at 470 nm followed by the shoulder peak at 433 and 412 nm. Upon addition of DMSO, the emission enhancement was observed with intensity maximum at 460 nm and 443 nm and followed by a shoulder at 410 nm. Upon increasing the DMSO concentration, emission maximum shifts to 457 nm and 442 nm followed by an emergence of new peak at 415 nm. Further increasing the volume of DMSO, a small peak at 414 nm was observed when compared with that of lower volume of DMSO [36]. The intensity of the emission peaks attained saturation upon increasing the concentration of DMSO. This enhancement of emission clearly suggests that the aggregation of complex takes place in the solvent mixture. The possible explanation can be the presence of adamantine group shields the Zn^{2+} ions thereby facilitating the emission enhancement. Whereas at high DMSO concentrations, the polarity of the solvents overcomes the shielding effect of adamantine and

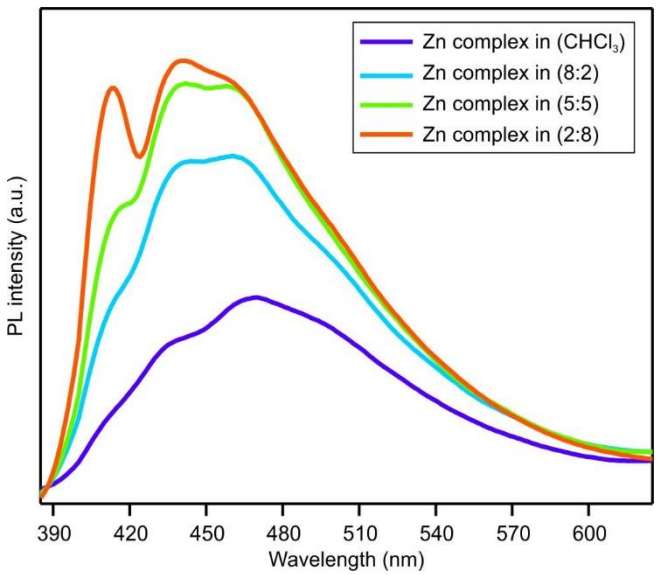

Fig. 12. Fluorescence spectra of ZnAADSB complex in mixture of $CHCl_3$ and DMSO solvents

coordinates with Zn metal ion. This coincides with quenching of emission. Furthermore, a DLS measurement also supports the increase in particle size upon increase in DMSO concentration (Fig. 13). The particle size of the zinc complex in chloroform shows 91 nm which increases to 148 nm upon increasing the DMSO concentration [37]. The particle size nearly doubled 283 nm when the chloroform and DMSO are in equal volume.

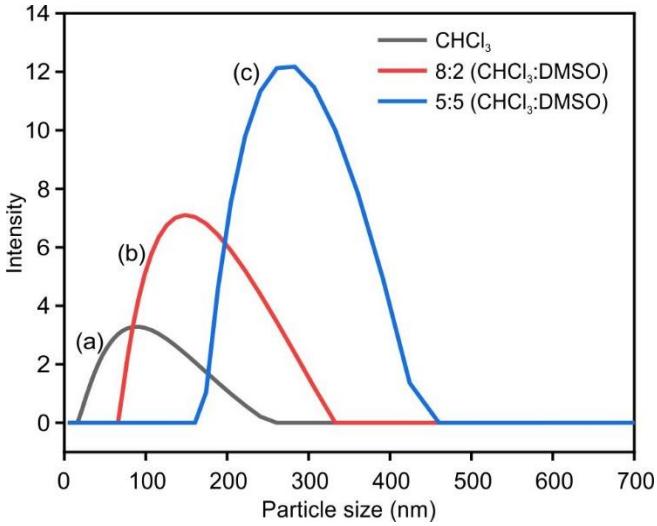

Fig. 13. DLS spectra of ZnAADSB complex in (a) $CHCl_3$ (b) 8:2 and (c) 5:5 in $CHCl_3$ and DMSO mixture

Photo-physical studies: The aggregation behaviour was studied by ^{1}H NMR using mixture of solvents used in photophysical studies using $CDCl_3$ and DMSO-d_6 solvents (Fig. 14). There happens to be a considerable change in the NMR spectra of Zn complex in the mixture of solvents as shown in electronic spectra. Similarly, when a coordinating solvent DMSO-d_6 were added, a new signal of imine protons at δ 8.520 ppm related to imine protons of aggregates. All the protons of both aromatic and aliphatic groups were downfielded with substantial broadening of peaks confirms the formation of aggregates along with free complex. Addition of the coordinating solvent did not favour the formation of DMSO adducts rather it facilitates the formation of aggregates which is unusual in

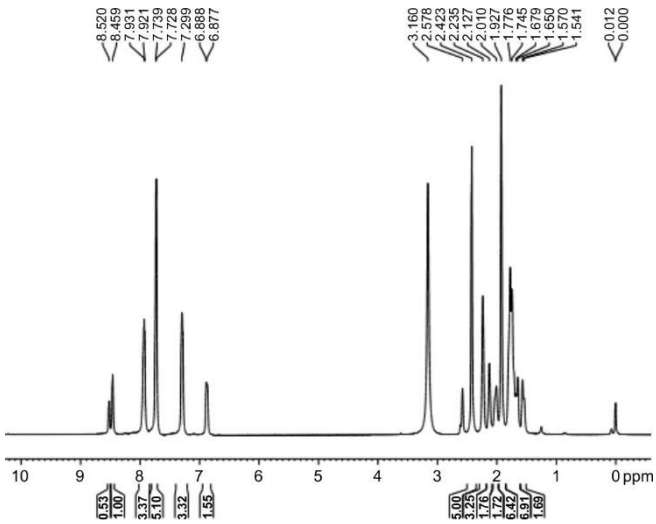

Fig. 14. Aggregated ^{1}H NMR spectrum of ZnAADSB complex in $CDCl_3$ DMSO-d_6 mixture

reported zinc complex containing with large alkyl groups. The possible explanation could be that the presence of large hydrophobic adamantine groups shields the Zn centre and restricts the DMSO from coordination at low concentration whereas the adduct could be possible at high DMSO concentration. This is in accordance with fluorescence quenching as observed in Fig. 12. This clearly indicates that the formation of aggregates is favoured in coordinating solvents which is in accordance with DLS data. The schematic representation of aggregation of ZnAADSB complex is shown in **Scheme-II**.

The ZnAADSB was irradiated using 365 nm light source continuously for 3 h and aliquot sample analysed by UV-Visible spectroscopy (Fig. 15). Before irradiation, the electronic spectrum of Zn complex shows the band due to n-π* transition of –C=N- at 365 nm and n-π* of azo group at 440 nm [38]. Upon exposure to 365 nm light, the electronic spectrum displays a *hypso* and hypochromic shift of a peak at n-π* transition and no change in n-π* of azo group. Furthermore, irradiation of the sample by visible light did not show any changes in absorbance spectrum. This clearly indicates the *trans-cis* isomerisation did not occur ever after 3 h. The bulky nature of adamantine group in the complex prevents rever-

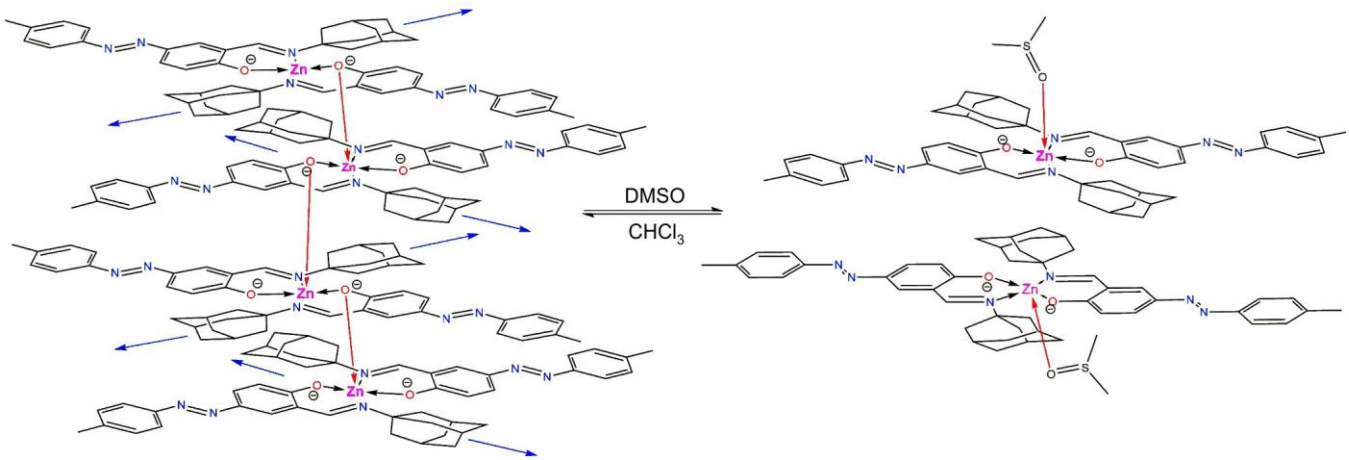

Scheme-II: Aggregation and de-aggregation of ZnAADSB complex

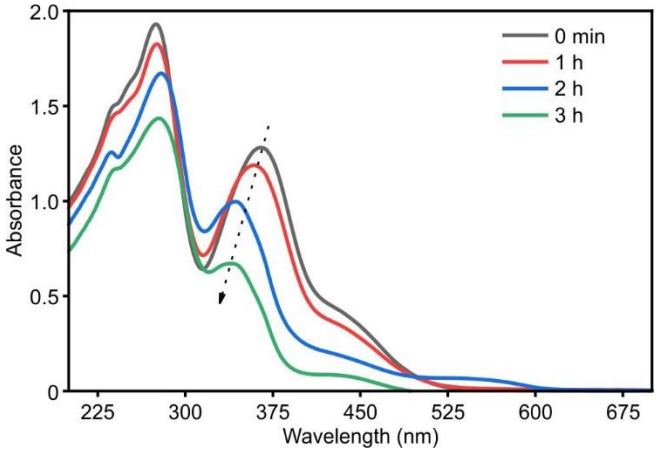

Fig. 15. UV-Visible spectral changes of ZnAADSB complex in $CHCl_3$ before and after irradiation at 365 nm light as a function of time

sible isomerisation process even irradiation for a prolonged time.

Antibacterial activities: The agar well diffusion assay was implemented to scrutinize the antibacterial efficacy of the synthesised ZnAADSB complex, coupled with its related ligand. The antibacterial efficiency of the ligand and its zinc complex was examined against Gram-negative (*E. coli*, *S. enterica*) and Gram-positive (*S. aureus*, *B. subtilis*) bacteria within a concentration range of 1000 to 100 μg/mL. The antibacterial activity of the ligand and its Zn complex was compared with ciprofloxacin as the standard drug.

The Zn complex showed higher activity than the free ligand against both Gram-positive and Gram-negative bacteria. At 1000 μg/mL, it produced inhibition zones of 22.37 ± 0.25 mm (*E. coli*), 21.47 ± 0.43 mm (*S. aureus*), 18.55 ± 0.31 mm (*S. enterica*) and 16.10 ± 0.17 mm (*B. subtilis*), whereas the ligand exhibited lower values under identical conditions. At 500 and 250 μg/mL, the Zn complex retained prominent activity, while the ligand showed reduced or no inhibition against some strains. The enhanced efficacy of the Zn complex may be due to increased lipophilicity after metal coordination, which improves membrane penetration and interaction with intracellular targets such as DNA gyrase [39-41].

The MIC and MBC concentrations revealed that the antibacterial efficacy of Zn complex was better compared to the ligand across all concentrations and bacterial strains tested. Fig. 16 showed the percentage of inhibition comparison graph of the ligand and complex. In contrast, the ligand showed lower inhibition rates of 89.42% for *B. subtilis*, 75.70% for *S. aureus*, 85.00% for *S. enterica* and 75.70% for *E. coli*. At lower concentrations, the Zn complex continued to function better; for example, at 250 μg/mL, it achieved inhibition rates ranging from 75.61% to 64.10%, whereas the ligand was less effective, achieving rates ranging from 69.82% to 60.63%.

The zinc complex demonstrated uniform antibacterial efficacy against *E. coli*, *S. aureus*, *S. enterica* and *B. subtilis*, evidenced by minimum inhibitory concentrations (MICs) of 500 μg/mL and the MBCs of 1000 μg/mL (Table-1) [42]. At a concentration of 1,000 μg/mL, the Zn complex inhibited *E. coli* (95.54%), *S. aureus* (90.52%), *S. enterica* (85.38%) and *B. subtilis* (80.86%) (Table-1). Except for *S. aureus*, where the MBC was >1000 μg/mL, the ligand showed similar MIC and MBC values. This difference suggests that the Zn complex possesses broader antibacterial activity or a stronger mode of action against the tested strains.

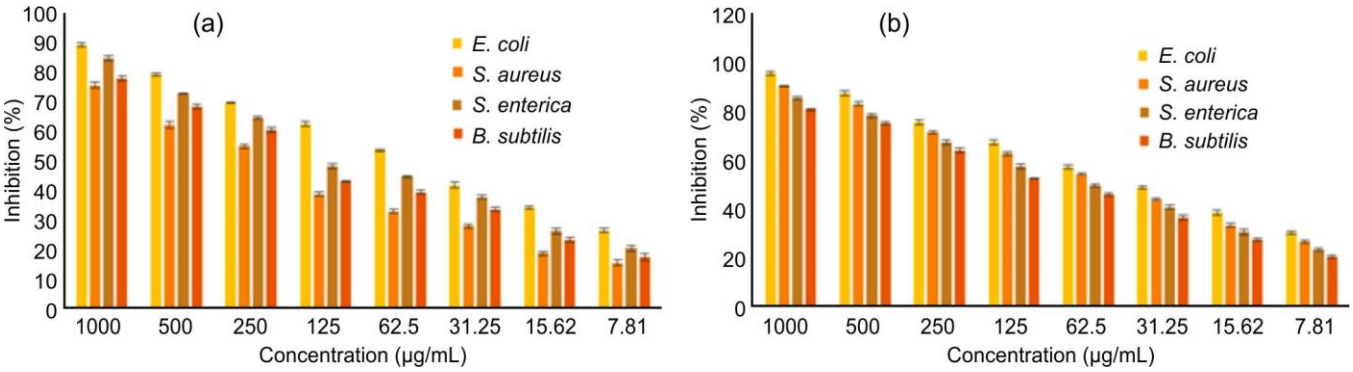

Fig. 16. Percentage of Inhibition comparison graphs of (a) ligand AADSB and (b) ZnAADSB complex

TABLE-1
PERCENTAGE INHIBITION OF ZnAADSB COMPLEX AND AADSB LIGAND

Conc. (μg/mL)	*E. coli*		*S. aureus*		*S. enterica*		*B. subtilis*	
	Zn complex	Ligand	Zn complex	Ligand	Zn complex	Ligand	Zn complex	Ligand
1000	95.54 ± 0.89	89.42 ± 0.71	90.52 ± 0.17	75.70 ± 1.06	85.38 ± 0.59	85.00 ± 0.86	80.86 ± 0.44	77.98 ± 0.86
500	87.54 ± 0.97	79.49 ± 0.52	83.05 ± 0.84	62.30 ± 1.17	78.33 ± 0.86	73.02 ± 0.21	75.22 ± 0.50	68.59 ± 0.85
250	75.61 ± 1.11	69.82 ± 0.33	71.51 ± 0.70	55.05 ± 0.68	67.37 ± 1.03	64.72 ± 0.65	64.10 ± 0.88	60.63 ± 0.86
125	67.35 ± 1.06	62.52 ± 0.86	62.74 ± 0.77	38.70 ± 0.70	57.49 ± 1.19	48.34 ± 0.79	52.40 ± 0.21	43.17 ± 0.21
62.5	57.17 ± 0.87	53.63 ± 0.42	54.32 ± 0.38	32.92 ± 0.65	49.65 ± 0.46	44.71 ± 0.28	45.84 ± 0.60	39.49 ± 0.60
31.25	48.86 ± 0.43	41.77 ± 1.05	44.11 ± 0.31	27.97 ± 0.64	40.70 ± 0.78	37.67 ± 0.66	36.48 ± 1.16	33.59 ± 0.68
15.62	38.67 ± 0.93	34.16 ± 0.56	33.38 ± 0.84	18.68 ± 0.68	30.72 ± 1.22	26.17 ± 1.12	27.46 ± 0.80	23.13 ± 0.86
7.81	30.55 ± 0.62	26.36 ± 0.68	26.63 ± 0.75	15.44 ± 0.97	23.44 ± 0.71	20.41 ± 1.01	20.60 ± 0.62	17.42 ± 1.07

Conclusion

An adamantane-based azo-Schiff base ligand (AADSB) and its corresponding Zn(II) complex (ZnAADSB) were successfully synthesized through a straightforward two-step route and comprehensively characterized by spectroscopic, analytical, morphological and thermal techniques. The spectral data confirmed effective coordination of zinc through the azomethine nitrogen and phenolic oxygen donor sites, leading to the formation of a stable metal complex with improved physico-chemical properties relative to the free ligand. The photophysical investigations demonstrated that ZnAADSB exhibits distinct solvent-responsive behaviour including aggregation-induced emission enhancement in chloroform/DMSO mixtures and fluorescence quenching at higher coordinating solvent content. These observations were supported by ^{1}H NMR and dynamic light scattering studies, which verified aggregate formation in solution. The absence of reversible photoisomerisation under UV irradiation suggests that the bulky adamantane framework restricts structural rearrangement of the azo chromophore. The biological evaluation revealed that zinc complexation significantly enhanced antibacterial activity against both Gram-positive and Gram-negative strains when compared with the parent ligand. The Zn complex consistently produced larger inhibition zones and more favourable MIC/MBC values indicating improved potency and broader antibacterial performance. This enhancement is likely associated with increased lipophilicity, better membrane permeation and stronger interaction with intracellular biological targets after metal coordination.

ACKNOWLEDGEMENTS

One of the authors, V. Veera Muthammal thanks to B.S. Abdur Rahman Crescent Institute of Science and Technology, Chennai, India, for the award of Junior Research Fellow under the University Fellowship (File No: Lr. No. 1738/Dean (R) 2024 Date: 23.09.2024).

CONFLICT OF INTEREST

The authors declare that there is no conflict of interests regarding the publication of this article.

DECLARATION OF AI-ASSISTED TECHNOLOGIES

During the preparation of this manuscript, the authors used an AI-assisted tool(s) to improve the language. The authors reviewed and edited the content and take full responsibility for the published work.

REFERENCES

1. A. Majumder, C. Sarkar, I. Das, S. Sk, S. Bandyopadhyay, S. Mandal and M. Bera, *ACS Appl. Mater. Interfaces*, **15**, 22781 (2023); https://doi.org/10.1021/acsami.2c21899
2. M.S. Kasare, P.P. Dhavan, B.L. Jadhav and S.D. Pawar, *ChemistrySelect*, **4**, 10792 (2019); https://doi.org/10.1002/slct.201901605
3. M. Pervaiz, S. Sadiq, A. Sadiq, U. Younas, A. Ashraf, Z. Saeed, M. Zuber and A. Adnan, *Coord. Chem. Rev.*, **447**, 214128 (2021); https://doi.org/10.1016/j.ccr.2021.214128
4. A.G. Imer, R.H.B. Syan, M. Gülcan, Y.S. Ocak and A. Tombak., *J. Mater. Sci.: Mater. Electron.*, **29**, 898 (2018); https://doi.org/10.1007/s10854-017-7986-z
5. F. Purtas, K. Sayin, G. Ceyhan, M. Kose and M. Kurtoglu, *J. Mol. Struct.*, **1137**, 461 (2017); https://doi.org/10.1016/j.molstruc.2017.02.065
6. V. Bressi, Z. Akbari, M. Montazerozohori, A. Ferlazzo, D. Iannazzo, C. Espro and G. Neri, *Sensors*, **22**, 900 (2022); https://doi.org/10.3390/s22030900
7. S. Slassi, M. Aarjane and A. Amine, *Appl. Organomet. Chem.*, **35**, e6408 (2020); https://doi.org/10.1002/aoc.6408
8. S. Samanta, A.A. Beharry, O. Sadovski, M. Theresa, A. Babalhavaeji, V. Tropepe, G.A. Woolley and S. Samanta, *J. Am. Chem. Soc.*, **135**, 9777 (2013); https://doi.org/10.1021/ja402220t
9. L. Thomas, I. Arbouch, D. Guérin, X. Wallart, C. Van Dyck, T. Mélin, J. Cornil, D. Vuillaume and S. Lenfant, *Nanoscale*, **13**, 6977 (2021); https://doi.org/10.1039/D1NR00106J
10. K.Y. Lam, C.S. Lee, M.R. Pichika, S.F. Cheng and R.Y.H. Tan, *RSC Adv.*, **12**, 15261 (2022); DOI https://doi.org/10.1039/D2RA01506D
11. M. Gaeta, I.P. Oliveri, G. Munzi, F.L. Presti and S. Di Bella, *Inorg. Chem.*, **63**, 3850 (2024); https://doi.org/10.1021/acs.inorgchem.3c04165
12. X. Xiao, Z.-J. Chen, R.J. Varley and C.-H. Li, *Smart Molecules*, **2**, e20230028 (2024); https://doi.org/10.1002/smo.20230028
13. N. Sinha, J. Wellauer, T. Maisuradze, A. Prescimone, S. Kupfer and O.S. Wenger, *J. Am. Chem. Soc.*, **146**, 10418 (2024); https://doi.org/10.1021/jacs.3c13925
14. M. Sugiura and H. Kandori, *Photochem. Photobiol. Sci.*, **23**, 1435 (2024); https://doi.org/10.1007/s43630-024-00602-w
15. T. Loan, M. Santra and M. Bradley, *Front Chem.*, **11**, 1205452 (2023); https://doi.org/10.3389/fchem.2023.1205452
16. Ö. Özdemir, *Turk. J. Chem.*, **43**, 266 (2019); https://doi.org/10.3906/kim-1807-24
17. D. Debnath, S. Roy, B.H. Li, C.H. Lin and T.K. Misra, *Spectrochim. Acta A Mol. Biomol. Spectrosc.*, **140**, 185 (2015); https://doi.org/10.1016/j.saa.2014.12.027
18. M. Khan, G.A. Nowsherwan, R. Ali, M. Ahmed, N. Anwar, S. Riaz, A. Farooq, S.S. Hussain, S. Naseem and J.R. Choi, *Molecules*, **28**, 1 (2023); https://doi.org/10.3390/molecules28247963
19. P. Ghosh, B.G. Roy, S. Jana, S.K. Mukhopadhyay and P. Banerjee, *Phys. Chem. Chem. Phys.*, **17**, 20288 (2015); https://doi.org/10.1039/C5CP02525G
20. F.J. Melendez, M.E. Castro, O. Portillo-Moreno, G. Hernández-Téllez, G.E. Moreno-Morales, D. Gutiérrez-Argüelles, R. Palomino-Merino, E. Rubio-Rosas and R. Gutiérrez-Pérez, *Molecules*, **24**, 3304 (2019); https://doi.org/10.3390/molecules24183304
21. L. Antonov, *Molecules*, **24**, 2252 (2019); https://doi.org/10.3390/molecules24122252
22. A. Koll, *Int. J. Mol. Sci.*, **4**, 434 (2003); https://doi.org/10.3390/i4070434
23. A.F. Santos, D.F. Brotto, L.R.V. Favarin, N.A. Cabeza, G.R. Andrade, M. Batistote, A.A. Cavalheiro, A. Neves, D.C.M. Rodrigues and A. dos Anjos, *Rev. Bras. Farmacogn.*, **24**, 309 (2014); https://doi.org/10.1016/j.bjp.2014.07.008
24. G.K. Ayyadurai, R. Jayaprakash, A. Shajahan and S. Rathika, *J. Biomol. Struct. Dyn.*, **43**, 2864 (2025); https://doi.org/10.1080/07391102.2023.2294383
25. K. Singh, M. S. Barwa and P. Tyagi, *Eur. J. Med. Chem.*, **41**, 147 (2006); https://doi.org/10.1016/j.ejmech.2005.06.006
26. G. Balachandran, A. Dhamotharan, K. Kaliyamoorthy, K.S. Rajammal, R. Kulandaiya and A. Raja, *Eng. Proc.*, **61**, 26 (2024); https://doi.org/10.3390/engproc2024061026
27. Ö. Özdemir, *J. Photochem. Photobiol. Chem.*, **392**, 112356 (2020); https://doi.org/10.1016/j.jphotochem.2020.112356
28. T.M. Shatir, K.A. Aly, M.M. Ebrahium, Y.B. Saddeek and E. Ranjith Kumar, *J. Mol. Liq.*, **401**, 124636 (2024); https://doi.org/10.1016/j.molliq.2024.124636

29. E. Ispir, M. Ikiz, A. Inan, A.B. Sünbül, S.E. Tayhan, S. Bilgin, M. Köse and M. Elmastaş, *J. Mol. Struct.*, **1182**, 63 (2019); https://doi.org/10.1016/j.molstruc.2019.01.029
30. G. Özkan, C. Kursun, H. Zengin, G. Zengin and M. Kurtoglu, *Transtion Met. Chem.*, **48**, 143 (2023); https://doi.org/10.1007/s11243-023-00531-0
31. S. Ramezanipoor, S. Parvarinezhad, M. Salehi, A.M. Grześkiewicz and M. Kubicki, *J. Mol. Struct.*, **1257**, 132541 (2022); https://doi.org/10.1016/j.molstruc.2022.132541
32. K. Buldurun, E. Tanış, N. Turan, N. Çolak and N. Çankaya, *J. Chem. Res.*, **45**, 753 (2021); https://doi.org/10.1177/1747519821995424
33. G. Ozkan, M. Kose, H. Zengin, V. McKee and M. Kurtoglu, *Spectrochim. Acta A Mol. Biomol. Spectrosc.*, **150**, 966 (2015); https://doi.org/10.1016/j.saa.2015.06.038
34. Y.Z. Xie, G.G. Shan, P. Li, Z.Y. Zhou and Z.M. Su, *Dyes Pigments*, **96**, 467 (2013); https://doi.org/10.1016/j.dyepig.2012.09.020
35. M. Maruthupandi and N.Y. Lee, *Chemosensors*, **12**, 180 (2024); https://doi.org/10.3390/chemosensors12090180
36. B. Das, M. Dolai, A. Dhara, S. Mabhai, A. Jana, S. Dey and A. Misra, *Anal. Sci. Adv.*, **2**, 447 (2021); https://doi.org/10.1002/ansa.202000165
37. M. Shyamal, P. Mazumdar, S. Maity, S. Samanta, G.P. Sahoo and A. Misra, *ACS Sens.*, **1**, 739 (2016); https://doi.org/10.1021/acssensors.6b00289
38. A. Kumar, R. Pandey, R.K. Gupta, V. Mishra, S.M. Mobin and D.S. Pandey, *Dalton Trans.*, **43**, 6365 (2014); https://doi.org/10.1039/c4dt00248b
39. R.S. Yamgar, Y. Nivid, S. Nalawade, M. Mandewale, R.G. Atram, and S.S. Sawant, *Bioinorg. Chem. Appl.*, **2014**, 276598 (2014); https://doi.org/10.1155/2014/276598
40. I. Wiegand, K. Hilpert and R.E.W. Hancock, *Nat. Protoc.*, **3**, 163 (2008); https://doi.org/10.1038/nprot.2007.521
41. N. Guo, Q.Y. Gai, J. Jiao, W. Wang, Y.G. Zu and Y.J. Fu, *Foods*, **5**, 73 (2016); https://doi.org/10.3390/foods5040073
42. M. Chandhru, R. Logesh, S. Kutti Rani, N. Ahmed and N. Vasimalai, *Environ. Technol.*, **43**, 3064 (2022); https://doi.org/10.1080/09593330.2021.1914181